energies

MDPI

Article

An Experimental Study on the Actuator Line Method with Anisotropic Regularization Kernel

Zhe Ma [1], Liping Lei [1,*], Earl Dowell [2] and Pan Zeng [1]

[1] Department of Mechanical Engineering, Tsinghua University, Beijing 100084, China; maz14@mails.tsinghua.edu.cn (Z.M.); zengp@mails.tsinghua.edu.cn (P.Z.)
[2] Department of Mechanical Engineering & Material Science, Duke University, Durham, NC 27704, USA; earl.dowell@duke.edu
* Correspondence: leilp@tsinghua.edu.cn; Tel.: +86-106-279-4261; Fax: +86-106-2771-279

Received: 19 January 2020; Accepted: 18 February 2020; Published: 21 February 2020

Abstract: Nowadays, actuator line method (ALM) has become the most potential method in wind turbine simulations, especially in wind farm simulations and fluid-structure interaction simulations. The regularization kernel, which was originally introduced to ALM to avoid numerical singularity, has been found to have great influence on rotor torque predictions and wake simulations. This study focuses on the effect of each parameter used in the standard kernel and the anisotropic kernel. To validate the simulation, the torque and the wake characteristics of a model wind turbine were measured. The result shows that the Gaussian width ϵ (for standard kernel) and the parameter in chord length direction ϵ_c (for anisotropic kernel) mainly affect the normal velocity of each blade element when using ALM but have little effect on the tangential velocity calculation. Therefore, these parameters have great influence on the attack angle and rotor torque prediction. The thickness parameter ϵ_t is the main difference between the standard kernel and the anisotropic kernel and it has a strong effect on the wind turbine wakes simulation. When using the anisotropic kernel, the wake structure is clearer and less likely to disperse, which is more consistent with the experimental results. Based on the studies above, a non-uniform mesh is recommended when using the anisotropic regularization kernel. Using a mesh refined in the main flow direction, ALM with anisotropic kernel can predict torque and wake characteristics better while maintaining low computational costs.

Keywords: actuator line method; wind turbine simulation; regularization kernel

1. Introduction

Nowadays, the actuator line method (ALM) has been widely used in wind farm simulations due to its capability of wind turbine wakes simulation and its numerical stabilization and low computational cost. This method was developed by Sørensen and Shen [1] in 2002 to overcome the disadvantage of Blade Element Momentum theory (BEM), which cannot simulate the wake characteristics of wind turbines. By combining the computational fluid dynamics (CFD) method and blade element theory, the ALM method avoids the calculation of the boundary layer flow and thus greatly reduces the computational cost compared with resolved CFD approaches. The benefits of low computational cost have two aspects. Firstly, the mesh used in ALM simulation is more regular than the resolved approaches, which means that the orthogonality of the mesh is much better. Therefore, the Large Eddy Simulation (LES) turbulence model, which is more accurate but computationally expensive and sensitive to mesh quality compared with RANS-based turbulence models, can be easily applied to ALM simulations. Combining with the LES model, ALM can make good simulations of velocity field and turbulence field in the wake region [2,3] and it has advantages in wind turbine simulations when the inlet condition is complex, such as the atmospheric boundary layer condition [4,5]. Secondly, due to

its low computational cost, ALM can be used in large-scale problems [4,6–8] and can be easily coupled with structural models [9,10]. Therefore, ALM is suitable for wind farm simulations and fluid-structure interaction simulations. In summary, ALM nowadays has become the most potential method in wind turbine simulations, especially in wind farm simulations and fluid-structure interaction simulations.

Regularization kernel was originally introduced to the ALM approach to avoid the numerical singularity [1]. During the ALM approach, the aerodynamic forces of wind turbine are calculated according to the blade element theory and the wind velocity field is calculated by solving the Navier–Stocks equations. Therefore, a regularization kernel must be employed to smoothly apply these aerodynamic forces to the Navier–Stocks equations and a uniform three-dimensional Gaussian function which is suggested by Sørensen and Shen [1] is widely used as the standard regularization kernel.

The regularization kernel also affects the conceptual shape of the wind turbine blade. When using the standard regularization kernel, the conceptual shape of a wind turbine blade will be like a cylinder [11], which is inconsistent with its real shape. Martínez-Tossas et al. [12] proposed a two-dimensional elliptical Gaussian function as the regularization kernel and its direction is based on the global coordinates. Churchfield et al. [13] developed an anisotropic Gaussian function as the regularization kernel whose direction is determined by the local coordinates of each blade element. By using these anisotropic kernels, the shaped of wind turbine blades can be better modeled, which will alleviate the need of tip correction and improve the simulation near the blade tip.

The gaussian width ϵ used in the regularization kernel was found to have great influence on rotor torque predictions, wake characteristics [2,14], and may cause new requirement for the mesh [15,16]. Troldborg states that the value of ϵ should be at least twice the local grid length to avoid numerical oscillation. Martínez-Tossas et al. [12] and Shives et al. [17] suggest that the value of ϵ should be a quarter of the local airfoil chord length. Shives also recommends limiting grid size to a quarter of ϵ. Churchfield et al. [13] states that ϵ should be around 0.035 times the rotor diameter when using the standard regularization kernel. Pankaj et al. [14] developed and tested a series of guidelines for choosing ALM parameters and the results showed that the appropriate ϵ should be determined by a function of blade aspect ratio, grid size and a empirical constant. As for the anisotropic kernel, Martínez-Tossas et al. [12] studied the influence of the chord length parameter ϵ_c and the thickness parameter ϵ_t for two dimensional flow and the result shows that $\epsilon_c \approx 0.4c$ and $\epsilon_t < 0.2$c are optimal. Churchfield et al. [13] studied the 3-dimensional wake characteristic of NREL (National Renewable Energy Laboratory) phase VI wind turbine with $\epsilon_c = 0.85c$, $\epsilon_t = 0.85t$ and simulations using the anisotropic kernel are more consistent with the experiment than the results of the standard kernel.

However, there is still confusion about the optimal value of the gaussian width and the effect of each parameter used in anisotropic kernel on ALM simulation result is still unclear. The recommended value of the gaussian width from the studies above do not agree with each other. Due to the author's experience, these recommended values of ϵ do not always lead to reliable results. Although the anisotropic kernel was developed in Churchfield's study [13], the parameters used in anisotropic kernel were not systematically studied. Furthermore, different parameters of $\epsilon_c = 0.4c$, $\epsilon_t = 0.2c$ were also used in this study for simulations of NREL 5MW wind turbine and the reason were not explained. Furthermore, the wake effect has great influence on the rotor torque of downstream wind turbines so the wake characteristics is significant in wind farm simulations and must be experimentally validated. In summary, the influence of the gaussian width used in regularization kernel and anisotropic kernel needs further study.

In this study, a new method is developed to measure the three-dimensional velocity field more efficiently and less expensively. Borrowing the idea of a frozen rotor, which is widely used in CFD simulations, the wake characteristics are reconstructed from the simultaneously gathered data of hot-wire anemometer and encoder. This measurement approach not only rebuilds the velocity distribution in a plane (along with or perpendicular to the main flow) but also reconstructs the whole wake region of a wind turbine. In this study, the influence of Gaussian width used in ALM with

anisotropic regularization kernel is studied. Validated by the experimental results of power and wake characteristics, the relationship among the parameters of the anisotropic regularization kernel, physical scale of the blade, and mesh grid size are determined. This relationship will be used in further studies of the coupled aeroelastic wake behavior of a wind turbine based on ALM.

2. Method

2.1. Actuator Line Method (ALM)

The actuator line method is realized using OpenFOAM which is an open-source computational fluid software. The Large Eddy Simulation (LES) turbulence model is employed in this study because of its accuracy in wake simulations. The equations are shown as Equations (1) and (2).

$$\frac{\partial \overline{u_i}}{\partial x_i} = 0 \tag{1}$$

$$\rho \frac{\partial \overline{u}_i}{\partial t} + \rho \frac{\partial \left(\overline{u}_i \, \overline{u}_j \right)}{\partial x_j} = -\frac{\partial p}{\partial x_i} + \frac{\partial}{\partial x_j} \left[\mu \left(\frac{\partial \overline{u}_i}{\partial x_j} + \frac{\partial \overline{u}_j}{\partial x_i} \right) \right] + \frac{\partial \tau_{ij}^s}{\partial x_j} + f \tag{2}$$

where $\overline{u}$ is the filtered velocity vector field, p is the scalar field of pressure, μ is a scalar represent the kinematic viscosity, $\tau_{ij}^s = -\rho \left(\overline{u_i u_j} - \overline{u}_i \, \overline{u}_j \right)$ is called the subgrid-scale (SGS) Reynolds stress [18], and the standard Smagorinsky SGS model is employed in this study.

f is the source term which represents the wind turbine blade forces in ALM. When considering the wind turbine blade as a series of blade elements, the force along the blade can be calculated according to Equation (3). Here C_l and C_d are the lift and drag coefficient, respectively. ρ is the density of air, v is the inlet velocity of the blade element, c is the chord length, and L is the length of the each blade element.

$$F_{element} = (F_l, F_d) = (\frac{1}{2} \rho v^2 c C_l L, \frac{1}{2} \rho v^2 c C_d L) \tag{3}$$

The forces calculated by Equation (3) are point forces and a regularization kernel must be employed to avoid a numerical singularity, as shown Equation (4). Traditionally, a uniform three-dimensional Gaussian function is employed as the standard regularization kernel in the actuator line method. ϵ is Gaussian width which adjusts the strength of this regularization kernel.

$$f = \sum F_{element} \otimes \eta_\epsilon \tag{4}$$

$$\eta_\epsilon = \frac{1}{\epsilon^3 \pi^{3/2}} \, \mathrm{e}^{-(\frac{r}{\epsilon})^2} \tag{5}$$

However, this uniform function will lead an imprecise approximation of the shape of the wind turbine blade. Although the chord length and the twist angle of the blade elements vary a lot from the root to the tip, the shape of the blade in actuator line model will be like a cylinder because of this uniform function. Furthermore, the uniform smooth function will cause the blade element force to be over concentrated along the chord direction, but more scattered along the thickness direction of the blade element at the meantime. Recently, an anisotropic regularization kernel as shown in Equation (6) was developed to overcome the disadvantages of the standard one.

$$\eta_\epsilon = \frac{1}{\epsilon_c \epsilon_t \epsilon_l \pi^{3/2}} \mathrm{e}^{-(\frac{r_c}{\epsilon_c})^2 - (\frac{r_t}{\epsilon_t})^2 - (\frac{r_l}{\epsilon_l})^2} \tag{6}$$

Here r_c, r_t, r_l are the distances between the grid center and the force point in local coordinates of each blade element and ϵ_c, ϵ_t, ϵ_l are the corresponding Gaussian widths. Figure 1 shows the influence range and the strength distribution of these two kernels, the blue curve represents the standard kernel and the red one represents the anisotropic kernel

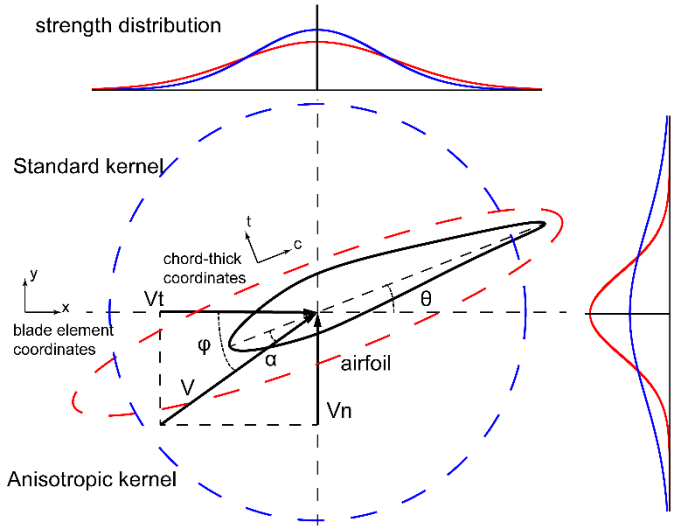

Figure 1. A schematic diagram of the influence range and strength distribution of two types of regularization kernel, the blue curve represents the standard kernel and the red one represents the anisotropic kernel.

2.2. Tip Loss Correction

Tip loss effect was first described by Prandtl who noted that the induced velocity tends to zero exponentially when approaching the blade tip and then the tip loss correction was introduced to BEM to make the simulation more realistic. For ALM, although the relationship between velocity and force is correct, a tip loss correction is suggested by Shen [19] due to the inconsistency between 2D airfoil data and attack angle of the 3D blade. This tip loss correction is employed in this study to compensate for the tip loss effect of wind turbine blade as shown in Equations (7) and (8).

$$F_1 = \frac{2}{\pi}\cos^{-1}[\exp(-g\frac{B(R-R_i)}{2R_i sin\phi_i})] \tag{7}$$

$$g = \exp\left(-0.125\left(\frac{B\Omega R}{U_\infty} - 21\right)\right) + 0.1 \tag{8}$$

Here, B is the number of blades, Ω is the angular velocity, ϕ_i is the inflow angle for the ith blade element. R and R_i are the radius of the rotor and the radial position of the ith blade element, respectively.

2.3. Simulation Setup

The dimension and boundary conditions are set up according to the experiment. The inlet velocity is 3.5 m/s. The calculation domain is shown in Figure 2. To get a better result for the wake characteristic, the potential wake region is refined. For the convenience of expression, the calculation domain is subdivided into two regions: the background region and the rotor & wake region. Figure 2 shows the details of the calculation domain. The calculation domain is a little longer than the wind tunnel to avoid the influence of the inlet condition. In summary, the calculation domain is 1.5 m by 1.5 m by 2.8 m and a wake region of 1.0 m by 1.0 m by 1.2 m is refined to get a better simulation of wake characteristics.

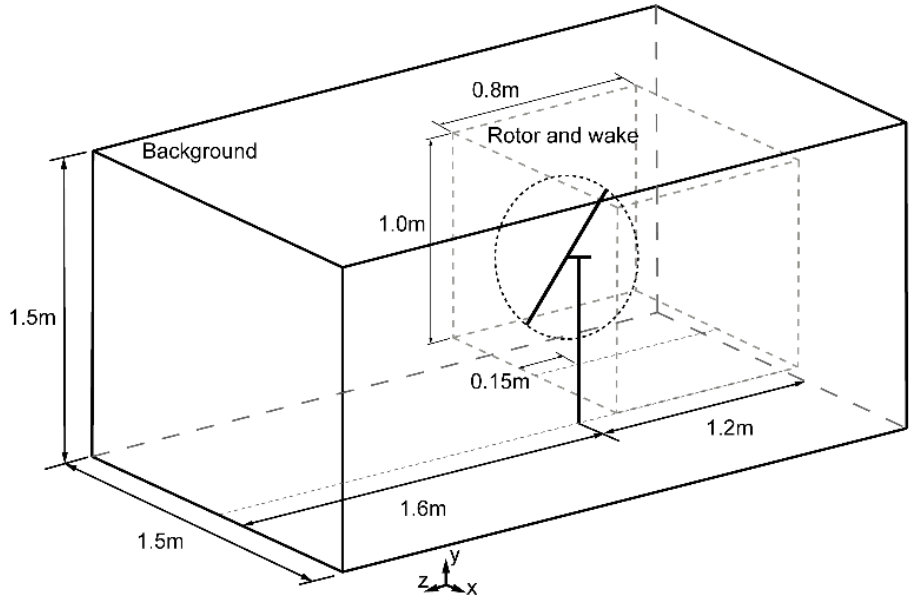

Figure 2. The calculation domain.

2.4. Experimental Setup

In this study, an experimental measurement of torque and wake characteristics was conducted to validate the simulations. Although Particle Image Velocimetry (PIV) technology has been proved to be powerful in wind turbine wake measurement [20–22], there are two restrictions for the PIV technology. When using the PIV system, the main direction of flow must be within the laser plane to guarantee that most of particles do not escape and stay illuminated. On the other hand, the measurement of the velocity field in three dimensions can only be achieved by using two cameras and a special laser generator [23,24]. The cost also constrains the use of PIV system. Due to these limitations of PIV system, hot-wire anemometer is also widely used in wake measurement. The wake experiments using hot-wire anemometer carried out by Schümann et al. [25], Lungo et al. [26], Singh et al. [27], and Dou [28] also made good measurements of wake characteristics. In this study, a new method for wind turbine wake measurement were developed using hot-wire anemometer.

Figure 3 shows the wind tunnel used in this experiment. It is composed of a contraction section, test section, diffuser section, and blower section. The length of the test section is 2.2 m and its cross-sectional dimensions are 1.5 m by 1.5 m. Equipped with three screens and two honeycombs and driven by four 11 kW mixed flow motors, the maximum velocity of the wind tunnel can reach 15 m/s and the turbulence intensity is around 0.5%.

A specifically designed two-blade wind turbine model is used in the experiment. The diameter of the rotor is 0.8 m and an NREL S826 airfoil profile is used all along the span for its high lift-drag ratio and low weight. The chord lengths and twist angles of the blade are shown in Figure 4.

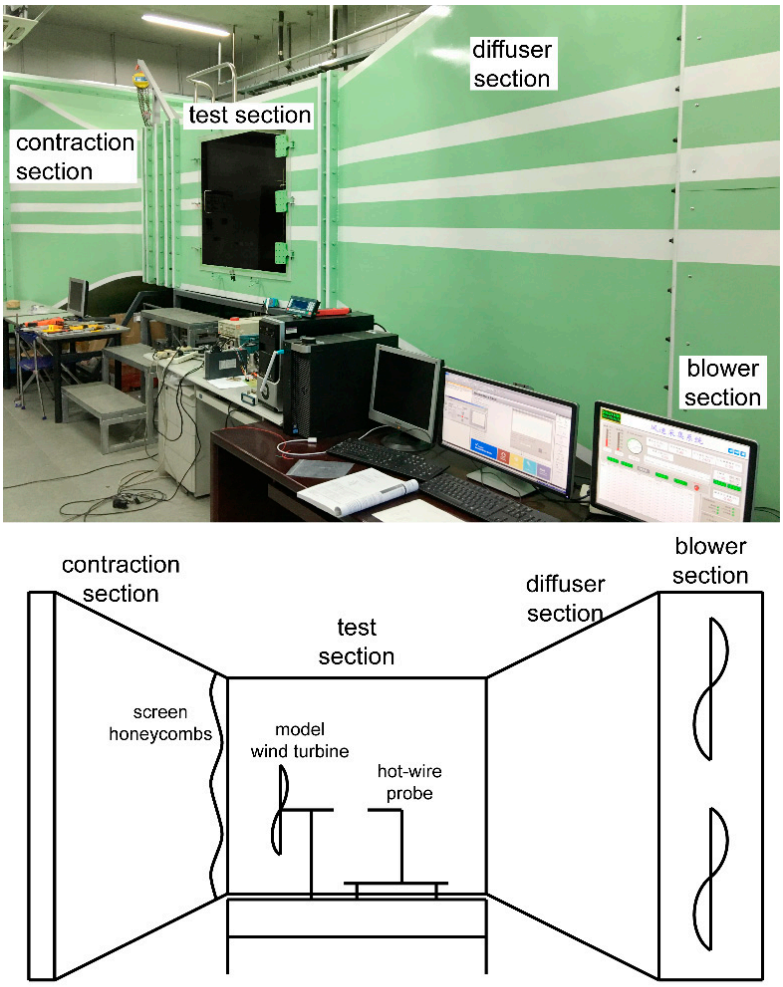

Figure 3. Wind tunnel used in experiment.

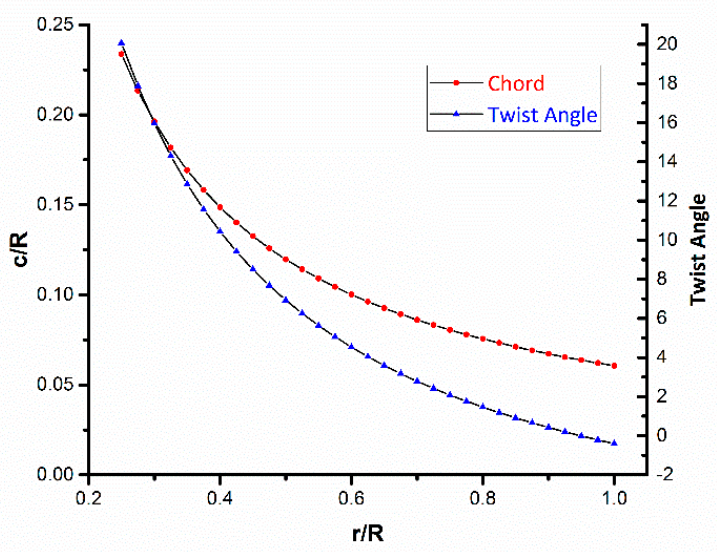

Figure 4. Length and twist angle distribution of the aerodynamics significant part of the blade.

The nacelle is equipped with an encoder of 1000 pulse, a torque sensor of 0.1% precision, and a servo-motor. This nacelle is designed mainly based on Anik's [29] equipment. During the experiment, the rotational speed of the rotor is totally controlled by the servo-motor and the relation between

aerodynamic force and the motor force can be determined by the sign of the torque data. The positive sign of the torque data indicates that the rotor is driven by wind and the serves as a load balancing. Furthermore, with this equipment, the friction of the whole system can be measured by a motor-driven experiment without blades. This can help to increase the precision of the experiment. The details of the wind turbine model are shown in Figure 5.

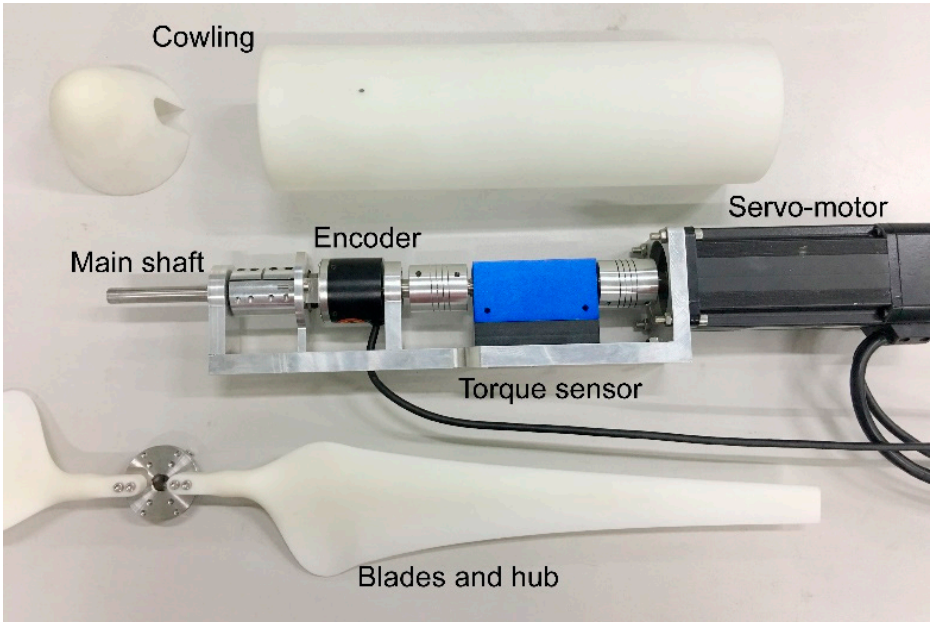

Figure 5. Wind turbine model and measurement equipment.

The inlet wind velocity is set to 3.5 m/s during the whole experiment. However, the rotational speed of the wind turbine model varies from 300 RPM to 650 RPM by 50 RPM. Thus, the tip speed ratio correspondingly varies from 3.6 to 7.8. For each rotational speed, the torque and wake characteristic of the model wind turbine are measured. It should be noted that the dimension and boundary condition of the simulation is strictly based on the experiment.

2.5. Frozen Rotor Method

Although PIV technology has been widely used in wind turbine experiments, it still has some limitations: the measuring plane must along the main flow direction to ensure the particle being illuminated, 2D-PIV can only measure the two-dimensional component of the wind field and 3D-PIV equipment is very expensive.

The frozen rotor method is widely used in CFD simulations for a rotating machine. When considering from the ground coordinates, the fluid field of a rotating machine is a transient problem. However, it can be turned into a static problem by considering form rotating coordinates. In this study, a new measurement method for wind turbine wakes was developed borrowing the idea of frozen rotor. A three dimensional hot-wire anemometer and encoder were employed to measure the velocity field in the wake region. At each measurement point, the wind velocity and the rotor azimuth were collected simultaneously. According to the axial symmetry of the wind turbine flow, this measurement can be considered as the hot-wire probe gathering velocity data around the axis of the rotor while the rotor and fluid field are frozen. Mean velocity was calculated according to the rotor azimuth to avoid the influence of small-scale vortex.

Figure 6 shows the experimental setup of hotwire anemometer probe. In this study, the probe was moved by an auto-controlled platform with the precision of 25 μm to scan a whole plane. Figure 7 shows all the locations of measured points. For each point, the wind velocity and encoder data are collected

simultaneously. Using the idea of frozen rotor, with each wind speed marked by a rotor azimuth, the wake characteristic can be reconstructed for the whole wake region. During the experiment, more measurement points were added to the potential tip vortex region, as shown in Figure 7, to get more precise results. By this way, we rebuild the wake region inexpensively but accurately with a hot-wire anemometer system.

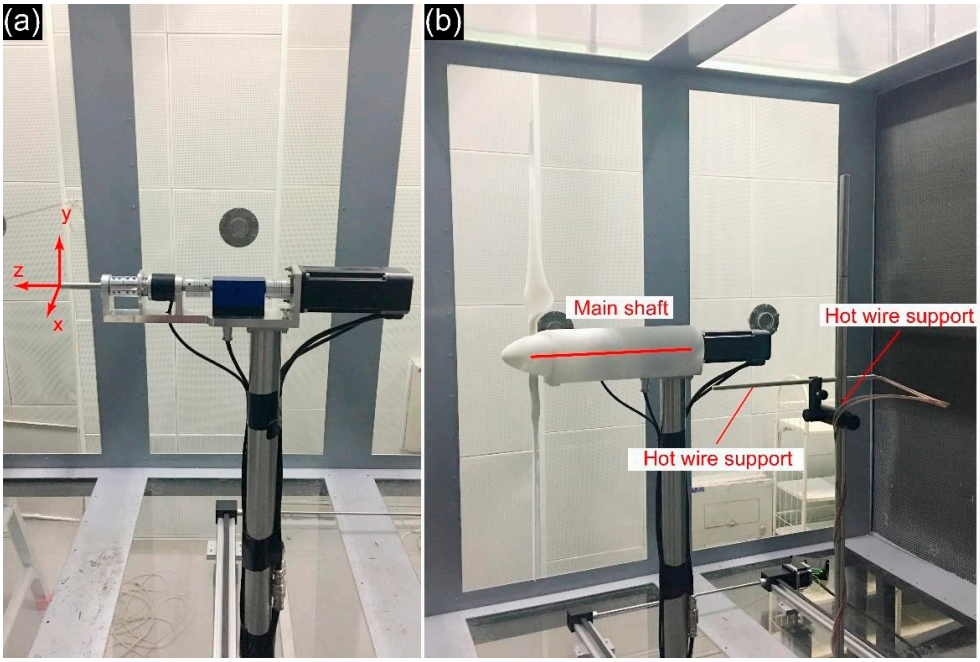

Figure 6. (**a**) Wind turbine model and coordinate system (**b**) hotwire anemometer probe location.

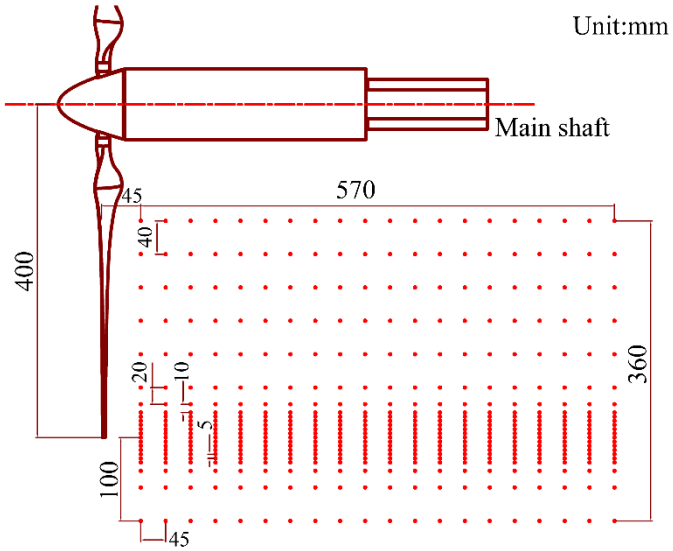

Figure 7. Locations of measurement points.

3. Result

3.1. Mesh Independence

Two levels of the mesh are compared to demonstrate the mesh independence of the simulation results of this study. Table 1 shows comparison of element number and element size between three mesh levels. The element size in the rotor and wake region is designed to be 10 mm in normal mesh

and 8 mm in refined mesh. Furthermore, a non-uniform mesh is specially designed to take advantage of the anisotropic kernel. The element size is 10 mm in rotor plane and 6 mm in the main flow direction.

Table 1. The comparison of element number and element size between three mesh levels (Unit: number of elements).

Mesh Level \ Region	Background	Rotor and Wake	Total Number	Element Size (Rotor and Wake)
Normal	228,608	800,000	1,112,108	10 mm, uniform
Refined	228,608	1,562,500	1,903,858	8 mm, uniform
Special	228,608	1,340,000	1,673,708	10 mm in rotor plane 6 mm in main flow direction

Figure 8 shows the torque result calculated by different meshes and different ϵ values, which are 16 mm, 20 mm, 24 mm, and 32 mm. Since the Gaussian $\epsilon > 2\Delta_{grid}$ must be guaranteed to avoid numerical oscillation, the torque result calculated with $\epsilon = 16$ mm is only achieved on the refined mesh. All results shown are calculated with the standard regularization kernel.

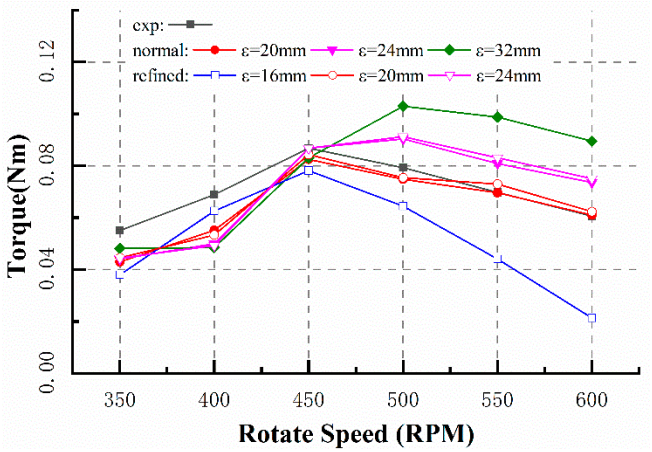

Figure 8. The comparison of torque result with different meshes and different ϵ values. Curves with the same color represent results using different level of mesh but the same Gaussian width.

The torque result shows that the normal mesh gives a similar prediction of the rotor torque compared with the results of the refined mesh when using the same ϵ value. Figure 9 shows the normal velocity (illustrated in Figure 1) of each blade element. It shows that normal mesh gives a similar prediction of the normal velocity compared with the results of the refined mesh. Therefore, it can be concluded that the simulations using a normal mesh are mesh independent.

It should be noticed that $\epsilon = 2\Delta_{grid}$ is not sufficient to guarantee a reliable simulation, because simulations with $\epsilon = 16$ mm and refined mesh give a totally different result compared with simulations with $\epsilon = 20$ mm and normal mesh. Furthermore, a rotating rotor generating torque is a physical phenomenon and it must not relate to the element size. On the other hand, Figure 8 also shows that the torque result is strongly affected by the ϵ value and does not going to converge when the ϵ value grows too much. This phenomenon will be discussed in the next section.

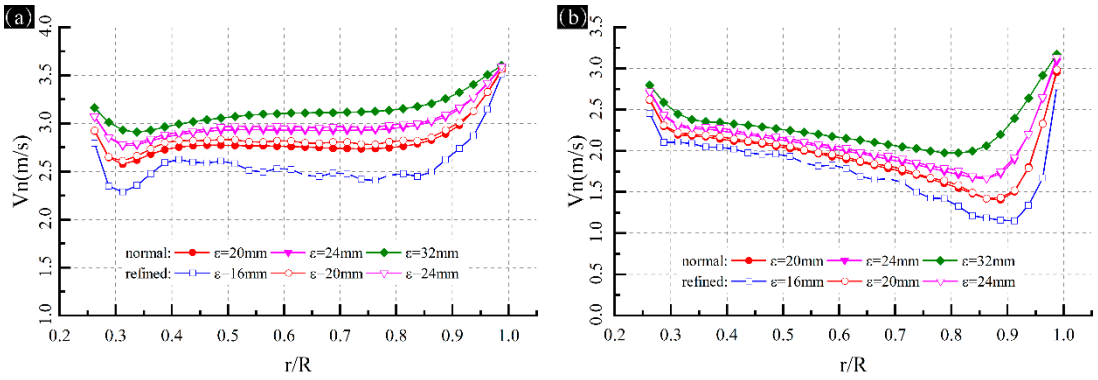

Figure 9. The normal velocity along the blade calculated by two levels of meshes with different Gaussian width when rotating speed is (**a**) 400 RPM, (**b**) 550 RPM. Curves with the same color represent results using the same Gaussian width but different level of mesh.

3.2. The Effect of Gaussian Width

In this section, the simulation results using different ϵ value are compared with the experimental results to study the influence of the Gaussian width. Figure 8 shows the comparison of the torque result between the experiment and simulations. According to the discussion above, the ϵ value is related to the chord length (chord length of blade tip when using standard regularization kernel) to make this study more referential. The lift and drag coefficient data obtained by Sarlak [30] are used in this study and the data were gathered at Re = 100,000, which is a little higher than the Reynolds number of this study. It should be noticed that the cross-section changes from a circle to airfoil S826 in the transition section of the model turbine blade and there are no aerodynamic data for this section and thus the aerodynamic performance of the transition section is neglected in all simulations. It is believed that the difference between the simulation result and the experimental result when rotating speed is 350 and 400 RPM is because of this neglecting. However, when the rotating speed increases, the contribution of the transition section to the aerodynamic load of the whole rotor can be neglected because it is close to the hub and its velocity is low. Nevertheless, the comparison illustrates that the prediction of torque does not converge when the ϵ value grows too much.

Figures 10 and 11 show the velocity and attack angle of each blade element when the rotating speed is 400 RPM or 550 RPM. It shows that the tangential velocity of different cases is almost the same when ϵ value varies and is mainly determined by the rotating speed of the rotor. However, the normal velocity is strongly affected by ϵ and the normal velocity increase with the value of ϵ. This has a significant influence on the attack angle of each blade element as shown in Figure 11 and therefore has a significant influence on the lift and drag force of each blade element. It should be noticed that the influence of the ϵ value on the torque result is not linear. According to the Reynolds number of this study, airfoil S826 gives the best aerodynamic performance when the attack angle is about 8 degree. Therefore, although the simulation with $\epsilon = 0.83c_{tip}$ gives a lower prediction of the normal velocity and the attack angle of each blade element, it gives a higher prediction of the torque, which shows a different trend compared with the results at other rotating speeds.

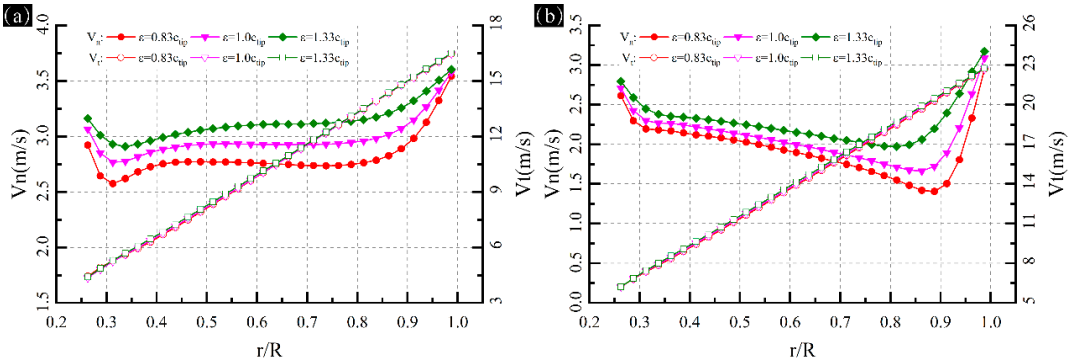

Figure 10. The V_n and V_t of each blade element along the blade when rotating speed is (**a**) 400 RPM, (**b**) 550 RPM.

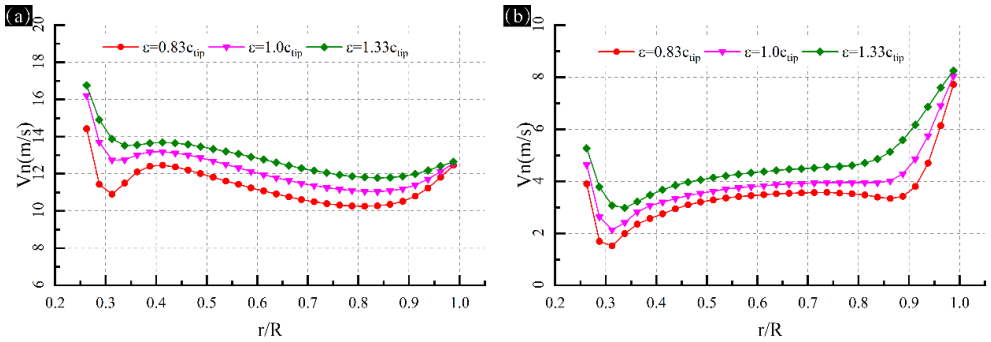

Figure 11. The attack angle of each blade element along the blade when rotating speed is (**a**) 400 RPM, (**b**) 550 RPM.

3.3. The Effect of the Chord Length Gaussian Width

Figure 12 shows the comparison for torque between experiment and simulations using the anisotropic regularization kernel. The best result using the standard regularization kernel is also added to the comparison. This figure also shows that the prediction of torque will not converge with the increment of the ϵc value. The empirical value of ϵ is not suitable for the anisotropic regularization kernel and $\epsilon_c = 1.2c$ shows the best prediction of the torque. However, the torque result is less sensitive to the ϵc value compared with the ϵ value when using standard regularization kernel. The simulation using anisotropic regularization kernel with $\epsilon_c = 1.0c$ also gives a reasonable enough prediction of torque.

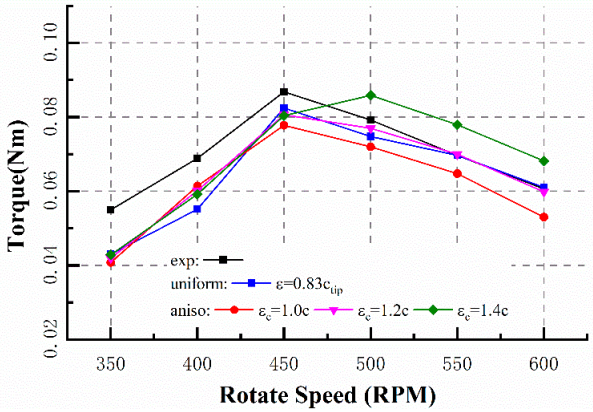

Figure 12. The comparison of torque between experiment, simulation using standard regularization kernel with $\epsilon = 0.83c_{tip}$, and simulations using anisotropic regularization kernel with different ϵ_c values.

The velocity and attack angle results when using anisotropic regularization kernel are different from the standard one. Figure 13 shows the comparison for the velocity between the result using standard regularization kernel with $\epsilon = 0.83c_{tip}$ and results using anisotropic regularization kernel with different ϵ_c values. It is clear that the tangential velocity of each blade element is less affected by the regularization kernel. However, the normal velocity is strongly affected by the regularization kernel which has been discussed. Compared with the result using anisotropic regularization kernel, the normal velocity is underestimated near the blade root and overestimated near the blade tip when using constant ϵ value. This matches with the previous discussion because the chord length of the blade root is larger than the tip one and a constant ϵ value will mispredict the affect region of a blade element. However, the attack angle of each blade element is not experimentally measured in this study due to the equipment limitation. Further study is needed to make a quantitative conclusion.

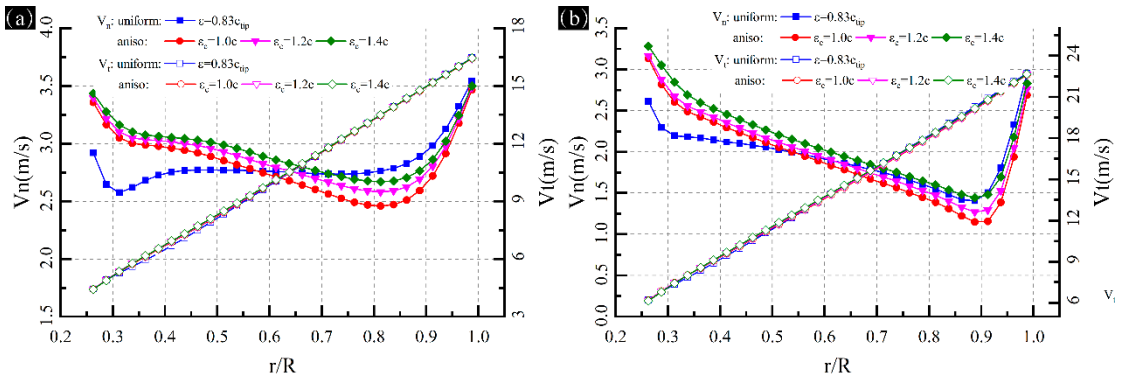

Figure 13. The V_n and V_t of each blade element along the blade when rotating speed is (**a**) 400 RPM, (**b**) 550 RPM.

According to the results above, although the optimal values are different, the effect of ϵ in standard kernel and the effect of ϵ_c in anisotropic is similar. Both ϵ and ϵ_c have little influence on the simulation result of tangential velocity, but will significantly affect the result of V_n and therefore significantly affect the rotor torque result. Figure 14 illustrates the effect region of different ϵ value. With a larger ϵ value, a blade element has a larger effect region in the actuator line method. However, the total value of the force is the same due to the Gaussian function, which means a regularization kernel has a flatter strength distribution when ϵ value is larger. Therefore, the regularization kernel with larger Gaussian width will affect a larger region of the flow and will lead to a higher velocity. This will cause an incorrect prediction of the attack angle of the blade element and has a strong effect on the prediction of lift and drag force.

It should be noticed that the optimal value in this study is different with the study of Martínez-Tossas [13] and Churchfield [12]. Actually, they do not agree with each other. Martínez-Tossas recommended $\epsilon = 0.14c \sim 0.24c$, Churchfield studied NREL 5MW wind turbine with $\epsilon_c = 0.4c$ and studied NREL Phase VI wind turbine with $\epsilon_c = 0.85c$ (here, c is the chord length). The main difference between these studies and this paper is the scale of the wind turbine. It could be inferred that the optimal parameters are related to the Reynolds number and this still needs further study.

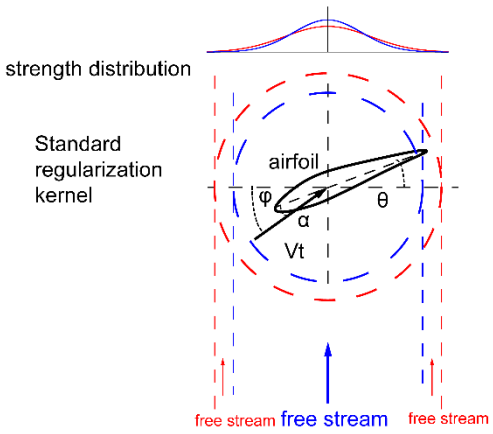

Figure 14. An illustration of the effective region of different ϵ value. The red one represents a regularization kernel with larger Gaussian width.

3.4. The Effect of the Thickness Gaussian Width

Table 2 shows the torque result when using different values of the thickness parameter ϵ_t. Since the thickness of the airfoil is much smaller than the chord length and usually smaller than the limit of $\epsilon > 2\Delta_{grid}$, the ϵt value is usually limited by an absolute value which is related to the grid size. Two different ϵ_t values are compared here. The series results for $\epsilon_t = 20$ mm are calculated on the normal mesh and this value is equal to twice of the grid size. The series results for $\epsilon_t = 9$ mm are calculated on the special mesh and this value is equal to 1.5 times of the grid size in the main flow direction. Table 2 shows that the thickness parameter has little influence on the torque results. Figure 15 shows the velocity component of each blade element and there is only a small difference for V_n which appears at the blade tip. It can be concluded that the thickness parameter ϵ_t has a little influence on the torque prediction of ALM.

Table 2. Torque result when using different ϵ_t value (Unit: Nm).

Speed	Exp	ϵ_c=1.2c, ϵ_t=20 mm	ϵ_c=1.2c, ϵ_t=9 mm
350	0.05504	0.04202	0.04291
400	0.06889	0.06014	0.05979
450	0.08679	0.08384	0.07998
500	0.07922	0.07701	0.07870
550	0.0697	0.07000	0.06982
600	0.06062	0.06228	0.06105

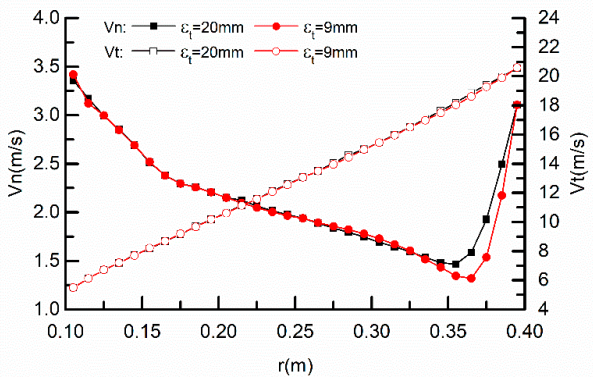

Figure 15. The V_n and V_t of each blade element along the blade when rotating speed is 500 RPM calculated by different ϵ_t value.

3.5. Wake Characteristic

Figure 16 shows the velocity distribution of the plane which is perpendicular to the main flow direction and 45 mm behind the rotor plane. The first row represents the experiment result, the second row represent the result of standard kernel and the third row represents the result of anisotropic kernel. The data area is a ring with outer radius of 500 mm and inner radius of 140 mm. The standard deviation as shown in Equation (9) is used to evaluate the difference between simulation and experimental result. Here, n is the number of sample points, v_{sim} is the simulation result and v_{exp} is the experimental result.

$$E = \sqrt{\frac{\sum_{i=1}^{n}\left(v_{sim} - v_{exp}\right)^2}{n v_{inlet}^2}} \tag{9}$$

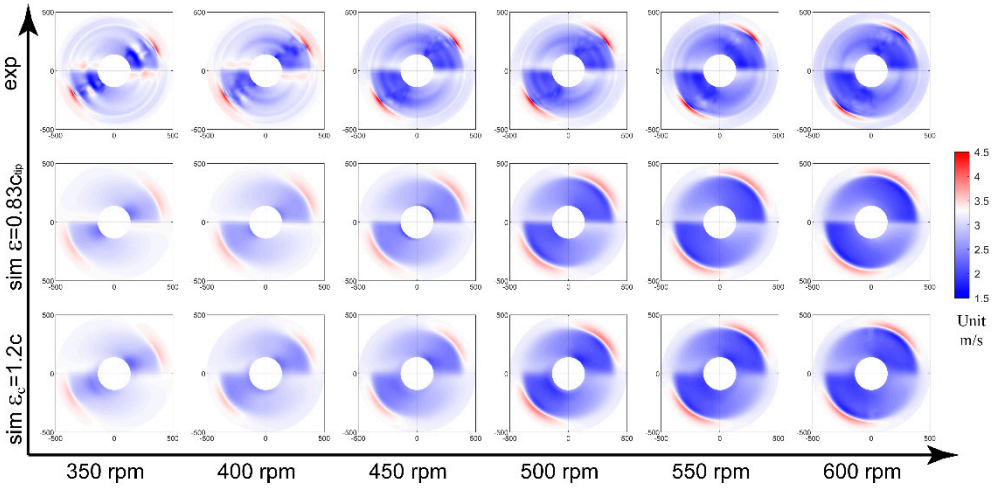

Figure 16. The velocity magnitude contour of the plane (45 mm behind the rotor) perpendicular to the main flow direction. The origin is the main shaft location and the data area is a ring with outer radius of 500 mm and inner radius of 140 mm. The first row represents the experiment result, the second row represent the result of standard kernel and the third row represents the result of anisotropic kernel.

As shown in Figure 17, the simulations show good agreement with the experimental result, the standard deviation between the simulation and experimental result is less than 6%. Furthermore, the standard deviation results illustrate that the ϵ value has little influence on the velocity distribution in the rotor plane.

Figure 18 shows the velocity distribution of the plane along with the main flow. The first row represents the experiment result, the second row represent the result of standard kernel and the third row represents the result of anisotropic kernel. The x coordinate represents the distance from the rotor plane and the y coordinate represents the radius position from the main shaft. The data area is from 45 mm to 615 mm behind the rotor and 140 mm to 500 mm away from the main shaft. The velocity distribution shows that the actuator line method can accurately simulate the pattern of the wake flow of a wind turbine. However, it also shows that the peak velocity of simulations is lower and the wake pattern is flatter compared with the experimental results. Figure 19 shows the standard deviation of velocity between simulations and experimental results. Although the improvement of velocity distribution is not significant, simulations with anisotropic regularization kernel show a more accurate result compared with simulations using the standard kernel.

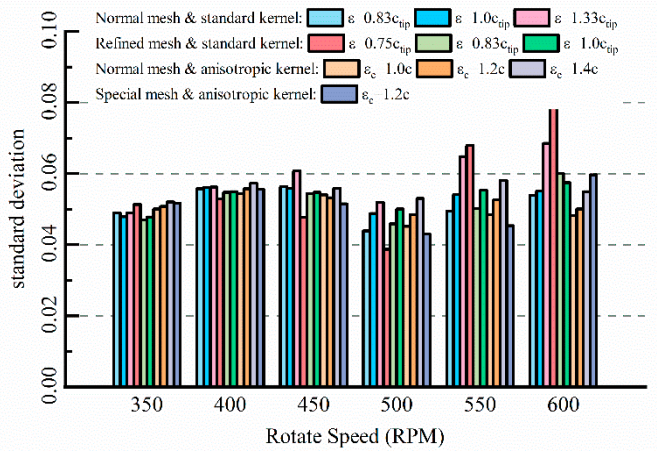

Figure 17. Standard deviation of the velocity magnitude in the plane perpendicular to the main flow direction.

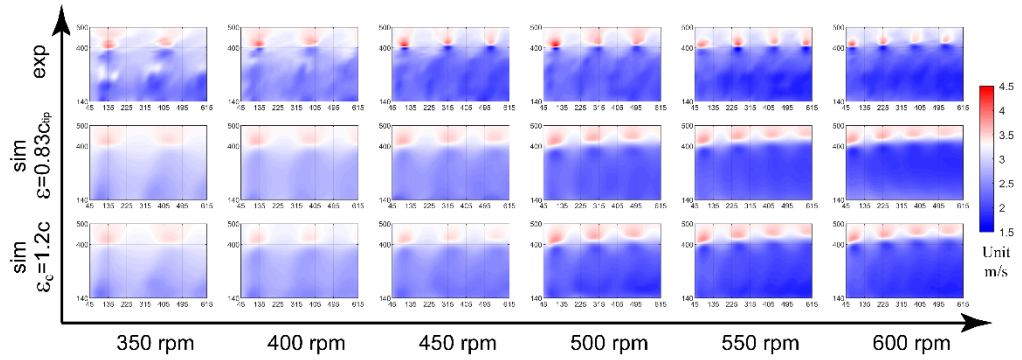

Figure 18. The velocity magnitude contour of the plane along with the main flow. The origin is the rotor center. The data area is from 45 mm to 615 mm behind the rotor and 140 mm to 500 mm away from the main shaft.

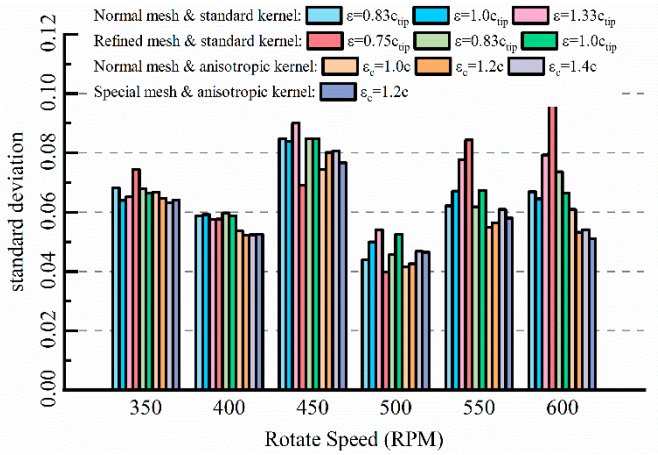

Figure 19. Standard deviation of the velocity magnitude in the plane along with the main flow.

Figure 20 shows the vorticity results. It is clear that the actuator line method gives a flatten prediction of the vorticity distribution because of the simplification of wind turbine blade. The peak vorticity of the experiment is much larger than the simulation result and the region of the high vorticity region is much smaller. However, the actuator line method gives a reliable prediction of the wake pattern. It is difficult to use standard deviation function to evaluate the vorticity results, because

both the position and the absolute value must be taken into consideration. Therefore, the correlation coefficient as defined in Equation (10) is used as the evaluation metric.

$$C = \frac{\sum \left(v_{sim} - \overline{v_{sim}}\right)\left(v_{exp} - \overline{v_{exp}}\right)}{\sqrt{\sum \left(v_{sim} - \overline{v_{sim}}\right)^2 \sum \left(v_{exp} - \overline{v_{exp}}\right)^2}} \tag{10}$$

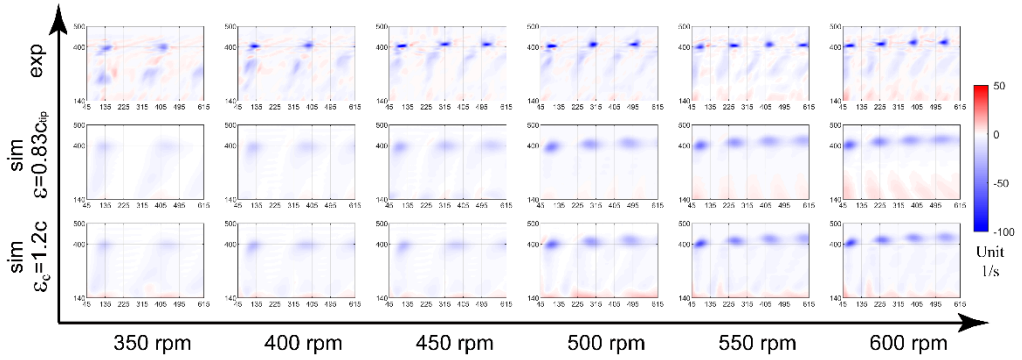

Figure 20. The vorticity magnitude contour of the plane along with the main flow. The origin is the rotor center. The data area is from 45 mm to 615 mm behind the rotor and 140 mm to 500 mm away from the main shaft.

The correlation coefficient neglects the average value difference between two distributions, but focuses on the pattern. In this study, the size of the high vorticity region and its position will significantly affect the correlation coefficient. Figure 21 shows the correlation coefficient between simulations and the experimental results. As the actuator line model predicts a flatter vorticity distribution, the correlation coefficient is not too good. However, simulations with a correlation coefficient higher than 0.5 give a reliable prediction of the position of high vorticity region, which means these simulations give a reliable prediction of the wake pattern. Furthermore, the correlation coefficient is significantly improved when using the anisotropic regularization kernel, especially when using the special mesh at the same time. As the main difference between the standard kernel and the anisotropic one is the thickness parameter, it can be concluded that the thickness parameter has a significant influence on the wake pattern prediction.

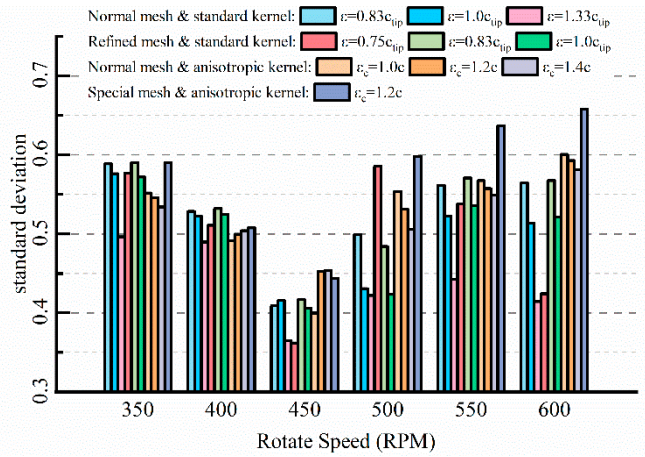

Figure 21. The comparison of the correlation coefficient.

It should be noticed that the number of elements of the special mesh is lower than the refined mesh, but the correlation coefficient of the simulations using the special mesh is much higher than

the simulations using refined mesh. These simulations obviously take the advantages of the anisotropic regularization kernel and significantly improve the performance of the actuator line model. A special mesh with refinement in the main flow direction together with the anisotropic regularization kernel will give a more accurate and lower computational cost simulation of the wind turbine.

4. Conclusions

In this paper, the mesh and parameters of the actuator line method with standard and anisotropic regularization kernel are studied. An experiment of the torque and wake characteristic was carried out, using hot-wire anemometer and borrowing the idea of frozen rotor method, to evaluate the simulation results. The relationship between Gaussian width ϵ, element size, attack angle of blade elements, and the simulation result of torque, and wake characteristic are discussed. The conclusion is as follows:

1. Gaussian width ϵ will strongly affect the torque result during actuator line simulations and it does not converge when ϵ becomes larger. Larger ϵ value will cause a higher prediction of the normal velocity of each blade element, but has little effect on the tangential velocity. The influence of the ϵ value on the attack angle is the main reason for its effect on the torque prediction.
2. In this study, $\epsilon = 0.83c_{tip}$ for standard regularization kernel and $\epsilon_c = 1.2c$ for anisotropic kernel can guarantee a reliable torque result. However, according to the state-of-art studies, the optimal value for ϵ varies with the scale of wind turbine. It can be inferred that the suitable parameters are related to the Reynolds number.
3. The thickness parameter ϵ_t has little influence on the torque prediction. However, the thickness parameter significantly affects the prediction of the wake characteristics. The anisotropic regularization kernel will improve the performance of the actuator line model in wake simulations.
4. Borrowing the idea of frozen rotor method, this study developed a reliable method to measure the wind turbine wakes. The wake characteristics were reconstructed by simultaneously gathered velocity data and rotor azimuth.
5. A special mesh with refinement in the main flow direction will take advantages of the anisotropic regularization kernel. Using a mesh refined in the main flow direction, ALM with anisotropic kernel can predict torque and wake characteristics better while maintaining low computational costs.

Author Contributions: Conceptualization, Z.M.; Formal analysis, Z.M.; Supervision, L.L. and P.Z.; Writing—original draft, Z.M.; Writing—review & editing, L.L., E.D. and P.Z. All authors have read and agreed to the published version of the manuscript.

Funding: This study was funded by National Natural Science Foundation of China (No.51875305) and Short-term Visiting Foundation of Tsinghua University (No.2018020).

Conflicts of Interest: The authors declare no conflict of interest.

Nomenclature

Variables

B	number of wind turbine blades
U_∞	free stream velocity [m/s]
Ω	rotor speed [rad/s]
R	rotor radius [m]
R_i	radial position of ith blade element
ϕ_i	inflow angle for ith blade element
η_ϵ	regularization kernel
ϵ	Gaussian width for standard regularization kernel [m]
ϵ_c	chord length Gaussian width for anisotropic regularization kernel [m]
ϵ_t	thickness Gaussian width for anisotropic regularization kernel [m]
ϵ_l	length Gaussian width for anisotropic regularization kernel [m]

ρ	air density [kg/m^3]
F_l	lift force [N]
F_d	drag force [N]
c	chord length [m]
L	length of blade element [m]
v	local velocity on blade element [m/s]
C_l	lift coefficient
C_d	drag coefficient
r	distance from the center of regularization kernel [m]
r_c	projection of r on the chord length direction of blade element [m]
r_t	projection of r on the thickness direction of blade element [m]
r_l	projection of r on the length direction of blade element [m]
E	standard deviation
C	correlation coefficient

References

1. Sorensen, J.N.; Shen, W.Z. Numerical modeling of wind turbine wakes. *J. Fluid. Eng.-Trans. ASME* **2002**, *124*, 393–399. [CrossRef]
2. Martinez-Tossas, L.A.; Churchfield, M.J.; Leonardi, S. Large eddy simulations of the flow past wind turbines: Actuator line and disk modeling. *Wind Energy* **2015**, *18*, 1047–1060. [CrossRef]
3. Mikkelsen, R.; Sørensen, J.N.; Øye, S.; Troldborg, N. Analysis of power enhancement for a row of wind turbines using the actuator line technique. *J. Phys. Conf. Ser.* **2007**, *75*, 012044. [CrossRef]
4. Lee, S.; Churchfield, M.J.; Moriarty, P.J.; Jonkman, J.; Michalakes, J. A Numerical Study of Atmospheric and Wake Turbulence Impacts on Wind Turbine Fatigue Loadings. *J. Solar Energy Eng.-Trans. ASME* **2013**, *135*. [CrossRef]
5. Storey, R.C.; Cater, J.E.; Norris, S.E. Large eddy simulation of turbine loading and performance in a wind farm. *Renew. Energy* **2016**, *95*, 31–42. [CrossRef]
6. Na, J.S.; Koo, E.; Munoz-Esparza, D.; Jin, E.K.; Linn, R.; Lee, J.S. Turbulent kinetics of a large wind farm and their impact in the neutral boundary layer. *Energy* **2016**, *95*, 79–90. [CrossRef]
7. Na, J.S.; Koo, E.; Jin, E.K.; Linn, R.; Ko, S.C.; Muñoz-Esparza, D.; Lee, J.S. Large-eddy simulations of wind-farm wake characteristics associated with a low-level jet. *Wind Energy* **2018**, *21*, 163–173. [CrossRef]
8. Zhong, H.M.; Du, P.G.; Tang, F.N.; Wang, L. Lagrangian dynamic large-eddy simulation of wind turbine near wakes combined with an actuator line method. *Appl. Energy* **2015**, *144*, 224–233. [CrossRef]
9. Ma, Z.; Zeng, P.; Lei, L.P. Analysis of the coupled aeroelastic wake behavior of wind turbine. *J. Fluids Struct.* **2019**, *84*, 466–484. [CrossRef]
10. Meng, H.; Lien, F.S.; Li, L. Elastic actuator line modelling for wake-induced fatigue analysis of horizontal axis wind turbine blade. *Renew. Energy* **2018**, *116*, 423–437. [CrossRef]
11. Sorensen, J.N.; Mikkelsen, R.F.; Henningson, D.S.; Ivanell, S.; Sarmast, S.; Andersen, S.J. Simulation of wind turbine wakes using the actuator line technique. *Philos. Trans. A Math. Phys. Eng. Sci.* **2015**, *373*, 20140071. [CrossRef] [PubMed]
12. Martinez-Tossas, L.A.; Churchfield, M.J.; Meneveau, C. Optimal smoothing length scale for actuator line models of wind turbine blades based on Gaussian body force distribution. *Wind Energy* **2017**, *20*, 1083–1096. [CrossRef]
13. Churchfield, M.J.; Schreck, S.J.; Martinez, L.A.; Meneveau, C.; Spalart, P.R. An advanced actuator line method for wind energy applications and beyond. In Proceedings of the 35th Wind Energy Symposium, Grapevine, TX, USA, 9–13 January 2017; p. 1998.
14. Jha, P.K.; Churchfield, M.J.; Moriarty, P.J.; Schmitz, S. Guidelines for Volume Force Distributions Within Actuator Line Modeling of Wind Turbines on Large-Eddy Simulation-Type Grids. *J. Solar Energy Eng. Trans. ASME* **2014**, *136*. [CrossRef]
15. Troldborg, N. Actuator Line Modeling of Wind Turbine Wakes. Doctoral Thesis, Technical University of Denmark, Lyngby, Denmark, 2009.
16. Troldborg, N.; Sorensen, J.N.; Mikkelsen, R.; Sorensen, N.N. A simple atmospheric boundary layer model applied to large eddy simulations of wind turbine wakes. *Wind Energy* **2014**, *17*, 657–669. [CrossRef]

17. Shives, M.; Crawford, C. Mesh and load distribution requirements for actuator line CFD simulations. *Wind Energy* **2013**, *16*, 1183–1196. [CrossRef]
18. Wu, Y.T.; Porte-Agel, F. Large-Eddy Simulation of Wind-Turbine Wakes: Evaluation of Turbine Parametrisations. *Bound.-Layer Meteorol.* **2011**, *138*, 345–366. [CrossRef]
19. Shen, W.Z.; Sørensen, J.N.; Mikkelsen, R. Tip Loss Correction for Actuator/Navier–Stokes Computations. *J. Solar Energy Eng.* **2005**, *127*, 209–213. [CrossRef]
20. Snel, H.; Schepers, J.; Montgomerie, B. The MEXICO project (Model Experiments in Controlled Conditions): The database and first results of data processing and interpretation. *J. Phys. Conf. Ser.* **2007**, *75*, 012014. [CrossRef]
21. Hong, J.; Guala, M.; Chamorro, L.; Sotiropoulos, F. Probing wind-turbine/atmosphere interactions at utility scale: Novel insights from the EOLOS wind energy research station. *J. Phys. Conf. Ser.* **2014**, *524*, 012001. [CrossRef]
22. Hong, J.; Toloui, M.; Chamorro, L.P.; Guala, M.; Howard, K.; Riley, S.; Tucker, J.; Sotiropoulos, F. Natural snowfall reveals large-scale flow structures in the wake of a 2.5-MW wind turbine. *Nat. Commun.* **2014**, *5*, 4216. [CrossRef]
23. Hu, H.; Wei, T.; Wang, Z. An Experimental Study on the Wake Characteristics of Dual-Rotor Wind Turbines by Using a Stereoscopic PIV Technique. In Proceedings of the 34th AIAA Applied Aerodynamics Conference, Washington, DC, USA, 13–17 June 2016; p. 3128.
24. Wang, Z.Y.; Ozbay, A.; Tian, W.; Hu, H. An experimental study on the aerodynamic performances and wake characteristics of an innovative dual-rotor wind turbine. *Energy* **2018**, *147*, 94–109. [CrossRef]
25. Schumann, H.; Pierella, F.; Saetran, L. Experimental investigation of wind turbine wakes in the wind tunnel. *Energy Procedia* **2013**, *35*, 285–296. [CrossRef]
26. Iungo, G.V.; Viola, F.; Camarri, S.; Porte-Agel, F.; Gallaire, F. Linear stability analysis of wind turbine wakes performed on wind tunnel measurements. *J. Fluid Mech.* **2013**, *737*, 499–526. [CrossRef]
27. Singh, A.; Howard, K.B.; Guala, M. On the homogenization of turbulent flow structures in the wake of a model wind turbine. *Phys. Fluids* **2014**, *26*, 025103. [CrossRef]
28. Dou, B.Z.; Guala, M.; Lei, L.; Zeng, P. Experimental investigation of the performance and wake effect of a small-scale wind turbine in a wind tunnel. *Energy* **2019**, *166*, 819–833. [CrossRef]
29. Anik, E.; Abdulrahim, A.; Ostovan, Y.; Mercan, B.; Uzol, O. Active control of the tip vortex: An experimental investigation on the performance characteristics of a model turbine. *J. Phys. Conf. Ser.* **2014**, *524*, 012098. [CrossRef]
30. Sarlak, H.; Mikkelsen, R.; Sarmast, S.; Sørensen, J.N. Aerodynamic behaviour of NREL S826 airfoil at Re= 100,000. *J. Phys. Conf. Ser.* **2014**, *524*, 012027. [CrossRef]